ADVANCED FUNCTIONAL MATERIALS
www.afm-journal.de

Nongeminate Recombination and Charge Transport Limitations in Diketopyrrolopyrrole-Based Solution-Processed Small Molecule Solar Cells

*Christopher M. Proctor, Chunki Kim, Dieter Neher, and Thuc-Quyen Nguyen**

Charge transport and nongeminate recombination are investigated in two solution-processed small molecule bulk heterojunction solar cells consisting of diketopyrrolopyrrole (DPP)-based donor molecules, mono-DPP and bis-DPP, blended with [6,6]-phenyl-C71-butyric acid methyl ester (PCBM). While the bis-DPP system exhibits a high fill factor (62%) the mono-DPP system suffers from pronounced voltage dependent losses, which limit both the fill factor (46%) and short circuit current. A method to determine the average charge carrier density, recombination current, and effective carrier lifetime in operating solar cells as a function of applied bias is demonstrated. These results and light intensity measurements of the current-voltage characteristics indicate that the mono-DPP system is severely limited by nongeminate recombination losses. Further analysis reveals that the most significant factor leading to the difference in fill factor is the comparatively poor hole transport properties in the mono-DPP system (2×10^{-5} cm^2 V^{-1} s^{-1} versus 34×10^{-5} cm^2 V^{-1} s^{-1}). These results suggest that future design of donor molecules for organic photovoltaics should aim to increase charge carrier mobility thereby enabling faster sweep out of charge carriers before they are lost to nongeminate recombination.

1. Introduction

Solution-processed small molecule bulk heterojunction solar cells (SSMBHSCs) with power conversion efficiencies (PCE) of 7% have recently been reported.[1] This achievement demonstrates that SSMBHSCs fabricated from blends of small molecule donors and fullerene acceptors are a viable alternative to polymer:fullerene based systems. However, despite the recent gains in efficiency several of the most efficient SSMBHSCs exhibit strong voltage dependent losses which limits both the fill factor (*FF*) and short circuit current (J_{sc}).[2–6] To date there have been few fundamental investigations into the recombination mechanisms that lead to these losses.[7,8] Significant improvements in PCE may result from a deeper understanding of the voltage dependent loss mechanisms within small molecule based photovoltaic systems.

The nature of the voltage dependent losses in polymer:fullerene based solar cells has been the subject of much research. There is evidence that poor charge transport properties,[9,10] geminate recombination[11–13] and both bimolecular (Langevin)[14–18] and trap-assisted (Shockley-Read-Hall)[19,20] recombination (nongeminate recombination) mechanisms may all play a role depending on materials and device processing conditions. Geminate recombination occurs when a coulombically bound electron-hole pair generated from absorption of a single photon recombines before the electron and hole can separate into free charge carriers. Nongeminate recombination is the recombination of free charge carriers and encompasses both trap-assisted and bimolecular mechanisms. Experimentally, geminate and nongeminate mechanisms can be distinguished by observing the timescale at which they occur and their dependence on carrier density. The probability of geminate recombination is independent of carrier density and geminate losses happen within nanoseconds of absorption.[8,11,13,17] In contrast, nongeminate losses are carrier density dependent and typically occur after micro-to milliseconds when illumination conditions are comparable to 1 sun.[14–16,18,21] Initial studies of SSMBHSCs based on diketopyrrolopyrrole (DPP) materials have concluded both geminate and nongeminate recombination can influence small molecule systems.[8] However, it is not known if this is true for all SSMBHSCs nor is it understood how these loss mechanisms can be overcome.

In this work, we study charge transport and voltage dependent recombination in two SSMBHSC systems consisting of DPP based donor molecules blended with [6,6]-phenyl-C71-butyric

C. M. Proctor, Dr. C. Kim, Prof. T.-Q. Nguyen
Center for Polymers and Organic Solids
University of California
Santa Barbara, CA 93106, USA
E-mail: quyen@chem.ucsb.edu
C. M. Proctor
Department of Materials
University of California
Santa Barbara, CA 93106, USA
Dr. C. Kim, Prof. T.-Q. Nguyen
Department of Chemistry and Biochemistry
University of California
Santa Barbara, CA 93106, USA
Prof. D. Neher
University of Potsdam
Institute of Physics and Astronomy
14476 Potsdam, Germany

DOI: 10.1002/adfm.201202643

© 2013 WILEY-VCH Verlag GmbH & Co. KGaA, Weinheim

acid methyl ester (PCBM). The first system 2,5-di-(2-ethylhexyl)-3,6-bis-(5″-n-hexyl–[2,2′,5′,2″]terthiophen-5-yl)–pyrrolo[3,4-c]pyrrole-1,4-dione (mono-DPP), has previously achieved a PCE of 3% when blended with PCBM despite a low *FF* of only 0.44.[4] The second system 4,7-bis{2-[2,5-bis(2-ethylhexyl)-3-(5-hexyl-2,2′:5′,2″-terthiophene-5″-yl)-pyrrolo[3,4-c]pyrrolo-1,4-dione-6-yl]-thiophene-5-yl}-2,1,3-benzothiadiazole (bis-DPP) was reported as a material with high ambipolar mobility in field effect transistors.[22] We first use single carrier diodes to gauge the hole and electron mobilities of each system. Impedance spectroscopy is then used to directly measure the voltage dependence of the series resistance and average charge carrier density. Additionally, we conduct effective carrier lifetime and light intensity measurements of operating solar cells to gauge the influence of nongeminate recombination. Compiling these data we are able to determine the physical origin of the difference in voltage dependence and accordingly a strategy for the future molecular design of high performing solution processed donor molecules for bulk heterojunction solar cells.

2. Results and Discussion

The mono-DPP:PCBM solar cell devices studied here averaged a 0.46 *FF*, 8.0 mA cm^{-2} J_{sc}, 0.75 V open circuit voltage (V_{oc}), and 2.8% PCE while the bis-DPP:PCBM devices averaged a 0.62 *FF*, 6.6 mA cm^{-2} J_{sc}, 0.51 V_{oc}, and 2.1% PCE (measured under AM1.5 irradiation 100 mW cm^{-2}). **Figure 1** shows the current density-voltage (*J–V*) response of typical devices measured along with the chemical structures of the mono- and bis-DPP materials (inset). The bis-DPP:PCBM system exhibits only minimal voltage dependent losses up until the V_{oc} while the mono-DPP:PCBM system features significant voltage dependent losses throughout the operating regime (from 0 V to V_{oc}). As discussed in the introduction, multiple processes could lead to this difference in voltage dependence. We will begin our analysis by exploring the charge transport properties of each system.

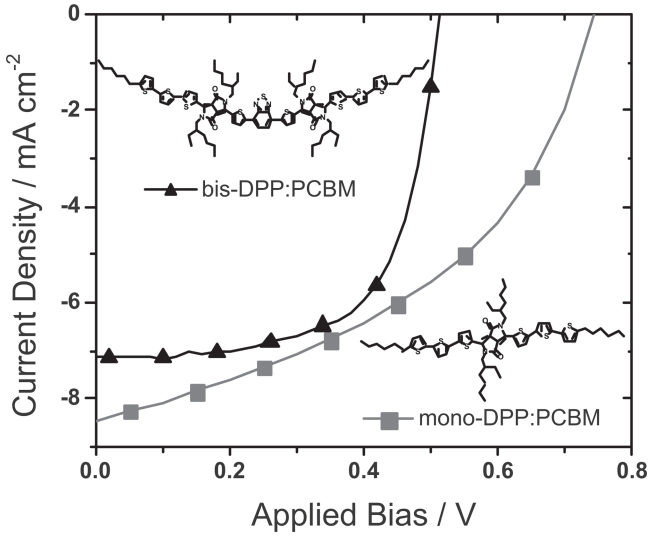

Figure 1. *J–V* characteristics of optimized bis-DPP:PCBM and mono-DPP:PCBM solar cell devices irradiated with 100mW cm^{-2} light intensity. Inset: chemical structure of bis-DPP and mono-DPP.

2.1. Charge Transport in Mono-DPP:PCBM and bis-DPP:PCBM Devices

The relation between charge transport and device performance in polymer:fullerene systems is well established.[9,10,23–25] If the hole and electron carrier mobilities are too low or heavily unbalanced, charges cannot be swept out efficiently before recombination resulting in low *FF*s and quantum efficiencies. In principal, it is expected that the same relations would hold for small molecule based solar cells thus we start our analysis by measuring the hole and electron mobilities in the optimized blend films. As mentioned above, bis-DPP was previously reported to have high field effect mobilities.[22] This demonstrates the material's efficient transport properties laterally but cannot be taken as a measure of the carrier mobility in a solar cell device, which occurs in the direction normal to the substrate. An initial estimate of the carrier mobilities of mono-DPP:PCBM devices was also reported;[4] however, these measurements were not confirmed across a range of film thicknesses. Here, the charge carrier mobilities in bis-DPP:PCBM and mono-DPP:PCBM blends are measured in a device geometry similar to solar cell devices for a range of thicknesses as shown in **Figure 2**a,b, respectively. The *J–V* characteristics of both electron-only (indium-tin-oxide (ITO)/Al/blend/Ca/Al) and hole-only (ITO/poly(3,4-ethylenedioxythiophene):poly(styrenesulfonate (PEDOT:PSS)/blend/Au) diodes show an excellent fit to the Mott-Gurney relation for space charge limited current:[26]

$$J = \frac{9\,\varepsilon_r \varepsilon_0\,\mu V^2}{8L^3} \quad (1)$$

where ε_r is the relative dielectric constant, ε_0 the permittivity of free space, μ the zero-field mobility and L the active layer thickness. The single-carrier devices for both systems demonstrate the L^{-3} dependence confirming that these devices truly exhibit space charge limited behavior. Using a relative dielectric constant of 4 as measured by impedance spectroscopy, the electron mobility, μ_e, of bis-DPP:PCBM is 150×10^{-5} cm^2 V^{-1} s^{-1} and the hole mobility, μ_h, is 34×10^{-5} cm^2 V^{-1} s^{-1}, a factor of 4.4 lower than the electron mobility. An equivalent measurement of single-carrier diodes with mono-DPP:PCBM reveals a significantly lower μ_h of only 2×10^{-5} cm^2 V^{-1} s^{-1}. Inclusion of a small field dependent term ($e^{\gamma\sqrt{V/L}}$ with $\gamma = 5.5 \times 10^{-5}$) was necessary for an accurate analysis of the current in the mono-DPP:PCBM electron-only devices yielding a μ_e of 100×10^{-5} cm^2 V^{-1} s^{-1}, a full 50 times higher than the hole mobility. That the mono-DPP:PCBM mobilities reported here are slightly different than previously reported may be attributable to a difference in processing conditions (80°C annealed in this study vs. as-cast in the previous report)[4] and to the influence of electrodes when the active layer is not sufficiently thick[28] (the previous report[4] used an 80 nm active layer). The similar μ_e observed in each system is consistent with the expectation that the μ_e in blend films should be comparable to the electron mobility of pristine PCBM films.[29,30]

The one order of magnitude lower hole mobility measured in the mono-DPP:PCBM diodes suggests that mono-DPP:PCBM

© 2013 WILEY-VCH Verlag GmbH & Co. KGaA, Weinheim

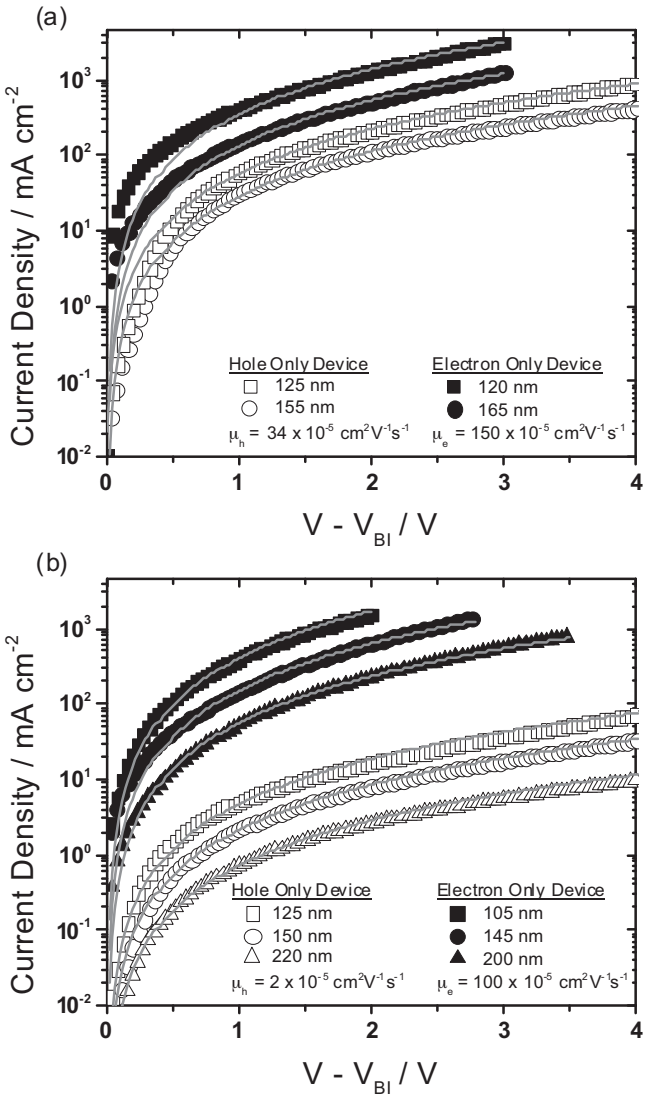

Figure 2. *J–V* characteristics of electron and hole only devices with a) bis-DPP:PCBM and b) mono-DPP:PCBM active layers. Grey lines are fits to Equation 1.

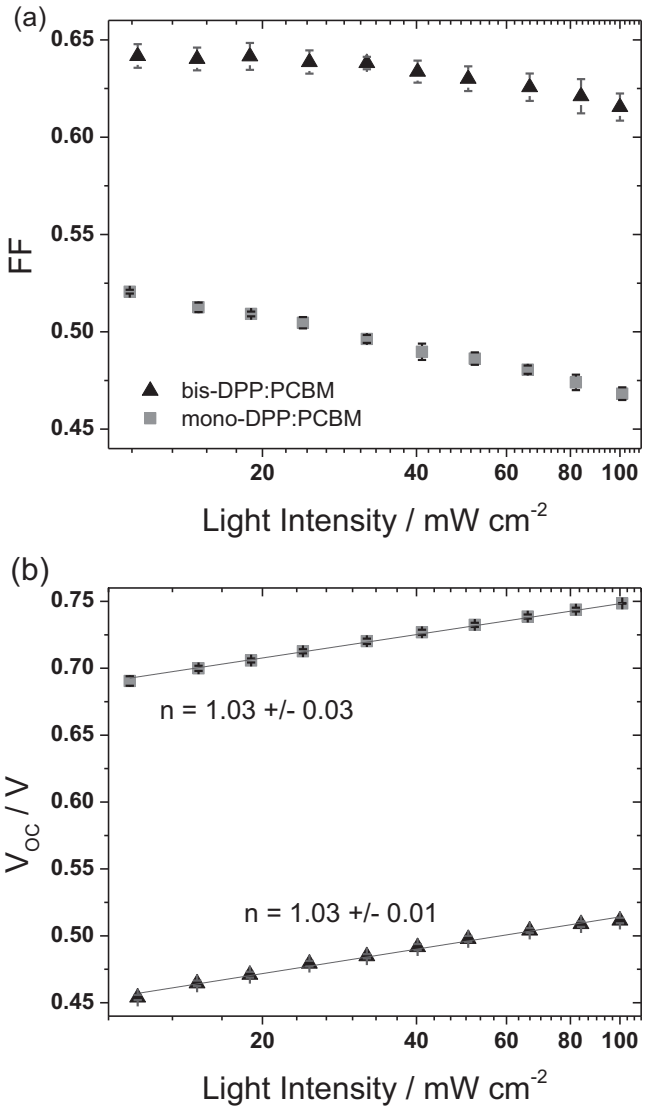

Figure 3. Light intensity dependence of a) *FF* and b) V_{oc} in bis-DPP:PCBM (triangles) and mono-DPP:PCBM (squares) solar cell devices.

solar cells may be transport limited. Nonetheless, the observation of lower charge carrier mobility alone is not sufficient evidence to conclude that the difference in voltage dependence observed in the mono-DPP:PCBM and bis-DPP:PCBM devices is solely an issue of charge transport. Geminate recombination or a short charge carrier lifetime (due to trapping or bimolecular recombination) could also contribute to the low *FF* observed in the mono-DPP:PCBM solar cells. Thus, further study of the recombination mechanisms is warranted.

2.2. Light Intensity Dependence of SMDPPEH:PCBM and BTDPP2:PCBM Solar Cells

Measuring the light intensity dependence of solar cell *J–V* characteristics has been demonstrated to be a powerful tool for probing the dominant recombination mechanisms.[9,25,31–33] Here we study the light intensity dependence of optimized mono-DPP:PCBM and bis-DPP:PCBM solar cell devices. The light intensity dependence of the *FF* and V_{oc} for each system are presented in **Figure 3** a and b respectively. The fact that the *FF* does not decrease at lower light intensities and that the V_{oc} shows a linear behavior over the entire intensity range in a semi-logarithmic plot can be held as an indication that the quality of the devices used in this analysis is good and the parasitical leakage current is sufficiently low. The *FF* of the mono-DPP:PCBM decreases with increasing light intensity as does the *FF* of the bis-DPP:PCBM system though not quite as significantly. To understand this trend, we first consider that the photogenerated charge carrier density scales with incident light intensity. Geminate recombination is independent of charge carrier density and consequently the probability of a geminate pair recombining should be independent of light intensity within the range studied here (0.1–1 sun). Nongeminate recombination in

© 2013 WILEY-VCH Verlag GmbH & Co. KGaA, Weinheim

contrast does depend on charge carrier density; for instance, an increase in charge carrier density would mean there is a greater probability of a free electron and hole "finding" one another and then recombining. Following this reasoning, the decrease in *FF* at higher light intensities is evidence that the *FF* of both systems is heavily influenced by nongeminate recombination at intensities close to 1 sun.[15,33]

Multiple studies have demonstrated that the light intensity dependence of the V_{oc} can provide insight into the role of trap-assisted recombination versus bimolecular recombination at the open circuit condition.[21,34] Both mono-DPP:PCBM and bis-DPP:PCBM exhibit a logarithmic dependence on light intensity ($V_{oc} \propto nkT/qln(P)$ where n is a constant, k is Boltzmann's constant, T is temperature, q is the elementary charge and P is the incident light intensity) with a slope of $\approx 1.0\ kT/q$. This indicates that trap states do not play a significant role at the open circuit condition in either of these systems. Thus as has been found for the majority of the polymer:fullerene systems,[19,32] bimolecular recombination dominates at open circuit in these SSMBHSCs.

In order to probe the recombination mechanisms away from open circuit the photocurrent (J_{ph}) for each system is analyzed as a function of bias and light intensity. For a system with negligible series resistance, $J_{ph} = J_L - J_D$, where J_L and J_D are the measured light and dark currents, respectively. **Figure 4** shows the J_{ph} of the bis-DPP:PCBM (a) and mono-DPP:PCBM (b) devices plotted versus the effective voltage ($V_{eff} = V_o - V_{ap}$) measured at several light intensities, where V_o is the voltage at which $J_{ph} = 0$ and V_{ap} is the applied bias. In the case of bis-DPP:PCBM, the photocurrent shows two primary regimes: a linear dependence on $V_o - V_{ap}$ and a regime in which the photocurrent quickly saturates ($V_{eff} \approx 1$V). The presence of only these two regimes suggests that this system has zero net trapped charge and the electric field is uniform throughout the active layer.[35] The photocurrent of the mono-DPP:PCBM system in contrast shows a stronger field-dependence across a large bias range not fully saturating until $V_{eff} \approx -5$ V. This can be explained in terms of the difference in charge carrier mobilities; the lower μ of mono-DPP:PCBM requires a stronger electric field to sweep out all of the photogenerated charges before they recombine. A complimentary possibility is that in mono-DPP:PCBM the separation of geminate electron-hole pairs can be assisted by a strong electric field. By this theory, the J_{ph} increases at higher effective voltage (reverse bias) because of a decrease in geminate recombination; however, analysis of the photocurrent alone cannot determine the influence of geminate recombination therefore an alternative approach is needed to evaluate this possibility.

Interestingly, despite the μ_h being 50 times less than the μ_e, the photocurrent in mono-DPP:PCBM does not appear to be space charge limited. Following the work of Goodman and Rose,[35] Mihailetchi et al.[9] showed that an imbalance in mobilities can lead to a buildup of space charge resulting in a photocurrent with a square root dependence on the effective voltage ($J_{ph} \propto V_{eff}^{1/2}$). We observe no significant bias range with such a dependence in mono-DPP:PCBM devices. Mihailetchi et al. also demonstrated that a space charge limited photocurrent scales with a three-quarters power dependence on light intensity. Figure 4c presents the light intensity dependence of J_{ph} in mono-DPP:PCBM and bis-DPP:PCBM devices measured at

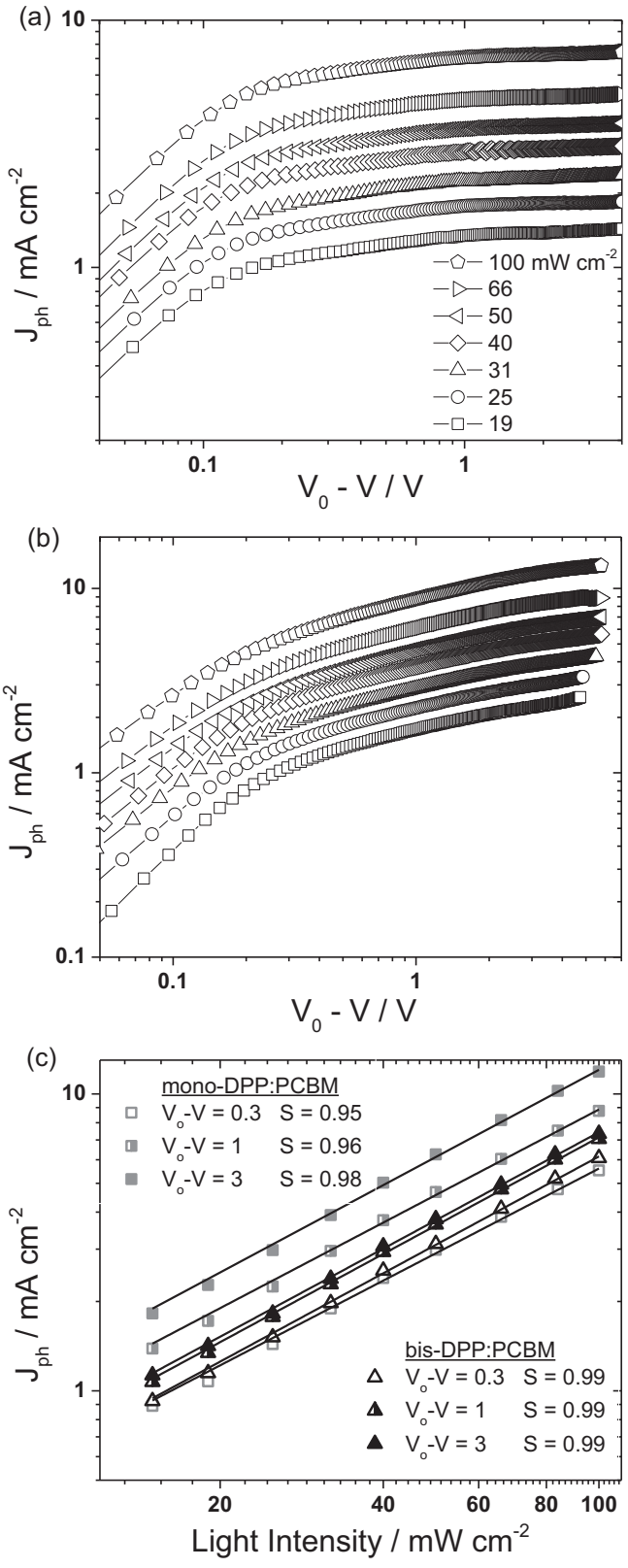

Figure 4. Photocurrent versus effective voltage in a) bis-DPP:PCBM and b) mono-DPP:PCBM solar cell devices. Light intensity dependence of the photocurrent in bis-DPP:PCBM and mono-DPP:PCBM solar cell devices with fit lines to $J_{ph} \propto P^S$.

© 2013 WILEY-VCH Verlag GmbH & Co. KGaA, Weinheim

different effective voltage conditions and fit to a simple power law relation $J_{ph} \propto P^S$. The J_{ph} in the mono-DPP:PCBM device does not approach the space charge limit of $S = 0.75$ even at lower effective voltages confirming that this system is not space charge limited. With that said, the slight sub-linear dependence of J_{ph} on light intensity indicates that space charge effects may still play a minor role. This sub-linear dependence could also be a sign of significant bimolecular recombination.[31]

It is worth noting that the linear light dependence seen for the J_{ph} in the bis-DPP:PCBM device should not be taken as evidence that there is no bimolecular recombination as has been done in other studies.[32,36] It has been shown that even systems dominated by bimolecular recombination can exhibit a J_{ph} with a linear dependence on light intensity up to 1 sun.[37,38]

To summarize the light intensity dependence results, it is evident that for both the mono-DPP:PCBM and bis-DPP:PCBM systems (i) bimolecular recombination dominates at open circuit and ii) the *FF* is heavily influenced by a nongeminate recombination mechanism. Based on the photocurrent analysis, the bis-DPP:PCBM system is nearly ideal with no evidence of trapping, space charge effects, or mobility limitations. In contrast, the J_{ph} in the mono-DPP:PCBM system shows a strong field dependence even at reverse bias conditions which is a direct result of the low hole mobility and may also be a sign of voltage dependent geminate recombination.

2.3. Impedance Analysis of Mono-DPP:PCBM and bis-DPP:PCBM Devices

To further understand the nature of the voltage dependent losses in mono-DPP:PCBM and bis-DPP:PCBM solar cell devices, differential resistance and capacitance analyses were conducted using an impedance analyzer. Impedance spectroscopy (IS) has been demonstrated to be a powerful tool for analyzing a variety of electronic devices including dye-sensitized solar cells,[39] light-emitting diodes[40,41] and more recently organic photovoltaics.[7,42–45] The advantage of impedance spectroscopy compared to other optoelectronic techniques is that impedance measurements are nondestructive and can be conducted at steady state for a range of bias conditions using standard device geometries and normal solar cell operating light intensities. Differential resistance analysis of impedance spectra also allows for a direct measurement of the series resistance which is crucial for an accurate characterization of the loss mechanisms in devices.[15,43,46]

In this study, the impedance response of mono-DPP:PCBM and bis-DPP:PCBM solar cell devices were measured at a range of DC bias conditions (–5 V to V_{oc}) and illumination intensities (0 to 100 mW/cm^2). For each bias and light condition, a constant DC bias was held across the illuminated device while the frequency of a 20 mV AC bias was swept from 50Hz–1.6MHz. A Cole-Cole plot of the impedance spectra from a representative mono-DPP:PCBM solar cell measured at an incident light intensity of 42 mW/cm^2 is presented in the **Figure 5**a. The symbols represent measured data points while the lines are fits to a simple RC circuit model (inset of Figure 5b). The circuit model used to fit the impedance spectra contains three elements: the series resistance (R_s), the device capacitance (C_u) and the differential diode resistance (R_{diff}). R_s represents the series resistance from both the experimental setup (cables and leads) and the device contacts. C_u originates from charges stored on the electrodes as well as the separation of positively charged donor (mono-DPP) domains and negatively charged acceptor (PCBM) domains within the photoactive layer. R_{diff} is a measure of the inverse slope of the *JV* curve at a given DC bias condition. As we will show, measuring R_s, C_u and R_{diff} as a function of DC bias allows for reconstruction of the *J–V* characteristics and determination of the series resistance corrected voltage scale and the average charge carrier density as a function of bias.

2.3.1. Series Resistance and Corrected Voltage Scale

As shown in Figure 5b, mono-DPP:PCBM exhibits a relatively small series resistance of ≈3 Ω cm^2 indicating that losses at the contacts are not the primary limitation to *FF*. The increase in R_s at higher V_{ap} suggests that the series resistance is influenced by charge injection from the contacts and may also capture some charge transport properties.[39,43,47] Measuring R_s as a function of bias allows for a precise correction of the voltage scale to account for the voltage drop due to the series resistance. The voltage drop due to the series resistance is $V_{Rs} = J_L A R_s$ where A is the electrode area. Thus, the actual voltage applied across the active layer is

$$V_{cor} = V_{ap} - V_{Rs}. \quad (2)$$

As this study is primarily concerned with losses occurring within the active layer, the subsequent analysis will make use of the corrected voltage scale (V_{cor}).

2.3.2. Differential Resistance and J–V Matching

With the corrected the voltage scale in hand, we can now consider the relation between R_{diff} and the *J–V* curve. Solar cells are not ohmic devices (i.e,. the current is not directly proportional voltage across the device) therefore the resistor R_{diff} is not ohmic in nature either. Rather, R_{diff} is a differential resistance which can be expressed as

$$R_{diff} = \left(\frac{dJ_L}{dV_{cor}} \right) \quad (3)$$

In words, R_{diff} is a measure of the inverse slope of the *J–V* curve at a fixed bias condition. Figure 5c displays the R_{diff} measured for a mono-DPP:PCBM device. As expected from Equation (3), R_{diff} decreases with forward bias consistent with the changing slope of the *J–V* curves. As the light intensity increases so too does R_{diff}. Similar to the FF light dependence, this can be explained by a carrier density dependent recombination mechanism (nongeminate recombination) that limits charge extraction more and more as carrier density increases. The R_{diff} dependence on light intensity decreases as V_{cor} approaches V_{oc} as injected carriers play an increasingly significant role in the recombination dynamics.

Using a similar circuit model analysis to characterize poly(3-hexylthiophene):PCBM devices, Boix et al. recently demonstrated that fitting R_{diff} to an exponential relation around $V_{cor} = V_{oc}$

© 2013 WILEY-VCH Verlag GmbH & Co. KGaA, Weinheim

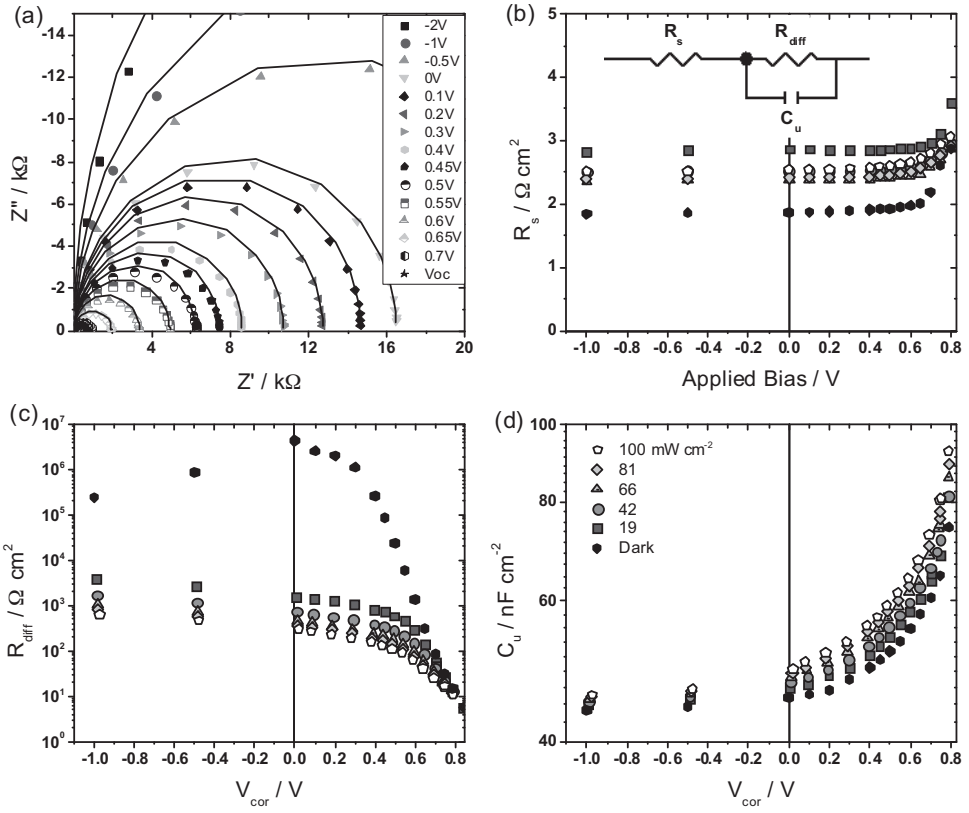

Figure 5. a) Measured impedance response of mono-DPP:PCBM device as a function of DC bias illuminated at 42 mW/cm^2 (symbols) and corresponding fits (lines) using circuit model (inset in (b)). b) Series resistance, c) R_{diff}, and d) C_u as a function of bias and light intensity extracted from circuit model fits.

allows for recreation of the *J–V* characteristics.[43] However, in contrast to their findings, in the case of mono-DPP:PCBM even with the decreasing light dependence of R_{diff} near V_{oc}, it is not observed that R_{diff} collapses to a single curve independent of light intensity. Furthermore, one observes there is some ambiguity in fitting an exponential relation to R_{diff} around V_{oc} depending on the bias range considered. Therefore, an alternative approach is needed to evaluate the influence of R_{diff} on the *J–V* characteristics.

A simple rearrangement of Equation (3) allows for a direct calculation of J_L from the measured R_{diff} values:

$$J_L(V_{cor}) = J_L(V_x) + \int_{Vx}^{V_{cor}} \frac{dV_{cor}}{R_{diff}} \quad (4)$$

where V_x determines the lower limit of the bias range and could in principal be set at any voltage less than V_{oc}. **Figure 6** shows the *J–V* characteristics for mono-DPP:PCBM as determined from R_{diff} using Equation (4) (symbols) align well with the *J–V* curve from the standard current voltage measurement (lines). The same procedure is also found to recreate the *J–V* characteristics with great precision for bis-DPP:PCBM and mono-DPP:PCBM devices with V_x = –5 V (see Supporting Information, Figure S1). Thus, the shape of the *J–V* curve from V_x to V_{oc} is clearly captured by R_{diff} as expected by the relation in Equation (3). This confirms the high quality of the impedance measurements.

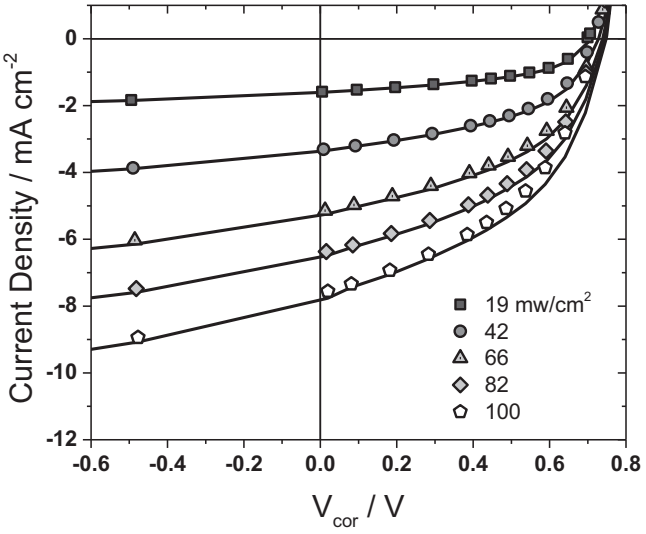

Figure 6. *J–V* curve from impedance data using Equation 4 (symbols) and measured *J–V* curves (lines) for mono-DPP:PCBM.

2.3.3. Capacitance and Average Charge Carrier Density

Having evaluated the resistive elements of the simple circuit model, we now turn to the capacitive element to determine the charge carrier density as a function of applied bias. The device

© 2013 WILEY-VCH Verlag GmbH & Co. KGaA, Weinheim

capacitance measured in a mono-DPP:PCBM device is plotted versus V_{cor} in Figure 5d. That C_u steadily increases with light intensity is strong evidence that it originates from photogenerated charges within the active layer. Notably, C_u also increases with forward bias in both illuminated and dark conditions. This implies that in addition to photogenerated charges, C_u is influenced by charge injection from the electrodes. Under reverse bias, where injection is minimal and most photogenerated charges are collected at the electrodes, C_u converges toward the geometrical capacitance (C_g). The device capacitance measured in the dark under appropriate reverse bias conditions (–1 V in this case) is precisely the geometric capacitance; for the mono-DPP:PCBM system this corresponds to a relative dielectric constant of ≈4.0.

To determine the average carrier density within in the active layer (n) from C_u, one must first account for the capacitive contribution from the electrodes. The internal capacitance originating from only photogenerated and injected charges (C_{in}) is then

$$C_{in} = C_u - C_g \tag{5}$$

Capacitance is the derivative of charge with respect to voltage thus it follows that

$$C_{in} = q\,AL\frac{dn}{dV_{cor}} \tag{6}$$

where q is the elementary charge and A is the electrode area. Rearranging Equation 6 and defining the carrier density at the saturation voltage to be n_{sat} leads to an expression for the carrier density as function of applied bias such that

$$n(V_{cor}) = n_{sat} + \frac{1}{q\,AL}\int_{V_{sat}}^{V_{cor}} C_{in}\,d\,V_{cor} \tag{7}$$

where V_{sat} is the voltage at which the photocurrent saturates. In principle, the lower limit for the integral in Equation 7 could start from any voltage (V_x) so long as $n(V_x)$ is known. The advantage of starting from V_{sat} is that n_{sat} can be determined directly from the impedance measured capacitance. Assuming that at V_{sat}, the generation rate is constant and recombination losses are negligible, it can be shown that

$$n_{sat} = \frac{1}{q\,AL}C_{sat}(V_0 - V_{sat}) \tag{8}$$

where C_{sat} is the internal capacitance measured at V_{sat} (see Supporting Information).

Having measured C_u from V_{sat} to V_{oc} we can now use Equations 5–8 to determine the average carrier density in mono-DPP:PCBM devices as a function of bias and light intensity (**Figure 7**a). As expected, the carrier density increases with both light intensity and applied bias. At open circuit, injected carriers account for approximately one third of the carrier density measured at 100 mW/cm^2. This observation is consistent with the findings of Shuttle et al. that the average charge carrier density in polymer:fullerene devices originates from both photogenerated charges and charges injected at the electrodes.[15]

Capacitances measured by impedance spectroscopy[7] and transient photovoltage in combination with transient photocurrent[48] have previously been used to determine the carrier density in an organic solar cell at open circuit. However, to the best of our knowledge, this is the first time IS measured capacitances have been used to determine the carrier density as a function of applied bias in an organic solar cell. To validate the technique the charge carrier density was also measured by a charge extraction technique (CE)[49] with a reverse extraction bias.[50] The carrier density measured by CE for a mono-DPP:PCBM device illuminated with LEDs at approximately one sun equivalent intensity is presented in Figure 7a (star symbols). The carrier density from CE agrees well with the impedance measured n within a reasonable variation attributable to device to device variations, deviations from the assumed uniform carrier density profile and limitations in the extraction technique arising from the imbalanced charge carrier mobilities.

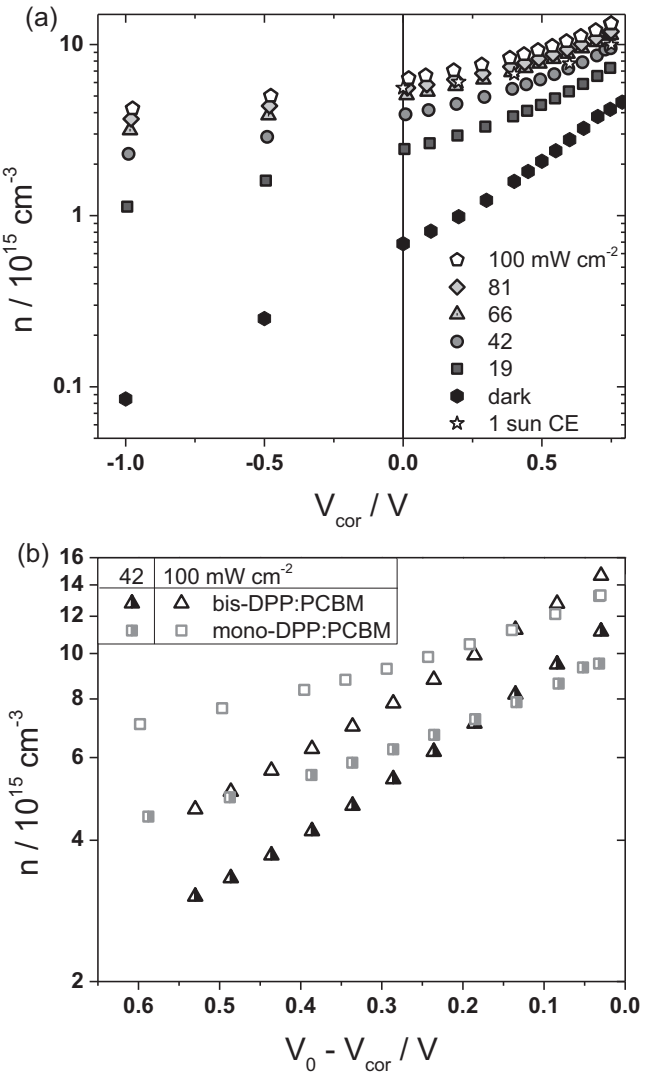

Figure 7. a) Charge carrier density versus the corrected voltage for the mono-DPP:PCBM system measured at different incident light intensities. The star symbols represent measurements made using a charge extraction technique. b) Charge carrier density versus effective voltage for mono-DPP:PCBM and bis-DPP:PCBM devices measured at 42 mW/cm^2 and 100 mW/cm^2.

© 2013 WILEY-VCH Verlag GmbH & Co. KGaA, Weinheim

Figure 7b presents the carrier density measured in bis-DPP:PCBM solar cells using the same impedance analysis alongside the n measured in mono-DPP:PCBM devices plotted versus effective voltage. The trend in n measured at effective voltages close to short circuit (0.78 V and 0.52 V for mono-DPP:PCBM and bis-DPP:PCBM, respectively) corresponds well with the respective short circuit currents. However, the n in the bis-DPP:PCBM system exhibits a steeper rise with forward bias leading to a carrier density at open circuit (n_{oc}) that is slightly greater than the n_{oc} measured in the mono-DPP:PCBM devices. This trend is indicative of comparatively weaker recombination in the bis-DPP:PCBM system consistent with the higher FF.

2.4. Recombination Current and Effective Carrier Lifetime

The impedance analysis in Section 2.3 measured the voltage dependence of the series resistance and the charge carrier density. Coupling this information with a simple analysis of the light current allows for estimation of the average time that a free charge carrier lives before recombining. This effective charge carrier lifetime, τ_{eff}, can be considered a measure of how fast recombination occurs: a longer τ_{eff} means photogenerated charges have more time to be swept out and collected at the electrodes before they are lost to recombination.

To determine τ_{eff} we first consider the recombination current, $J_{rec,}$ which by definition is the current lost to recombination at any given bias condition. When the light current saturates, recombination losses are negligible meaning J_{rec} (V_{sat}) = 0 and J_L (V_{sat}) = J_{sat}, thus it follows that:

$$J_{rec}(V_{cor}) = J_{sat} - J_L(V_{cor}). \quad (9)$$

In principle, J_{rec} encompasses all recombination loss mechanisms that can cause a small change in current - both geminate and nongeminate. With that said, it is clear from the light intensity measurements in Section 2.2 that both systems considered here are heavily influenced by nongeminate recombination losses at 1 sun incident light intensity. This suggests that J_{rec} at 1 sun is primarily a measure of the nongeminate recombination current. Therefore our subsequent analysis will assume that voltage dependent geminate losses are negligible. A discussion of the case in which geminate losses are more significant is included in the Supporting Information.

If J_{rec} is purely nongeminate recombination it can be expressed as

$$J_{rec}(V_{cor}) = q\,L\,\frac{n(V_{cor})}{\tau_{eff}(V_{cor})} \quad (10)$$

where τ_{eff} may be influenced by charge trapping and/or bimolecular recombination. As we have already measured $n(V_{cor})$ and $J_{rec}(V_{cor})$, $\tau_{eff}(V_{cor})$ can be extracted from the relation in Equation (10). The effective charge carrier lifetime in mono-DPP:PCBM and bis-DPP:PCBM devices measured at 1 sun incident light intensity is presented as a function of effective voltage in **Figure 8**. For $V_0 - V_{cor} > 0.2$ V, the τ_{eff} in bis-DPP:PCBM is more than three times that measured in mono-DPP:PCBM which means that on average charge carriers recombine at least three times faster in the mono-DPP:PCBM system. This is consistent

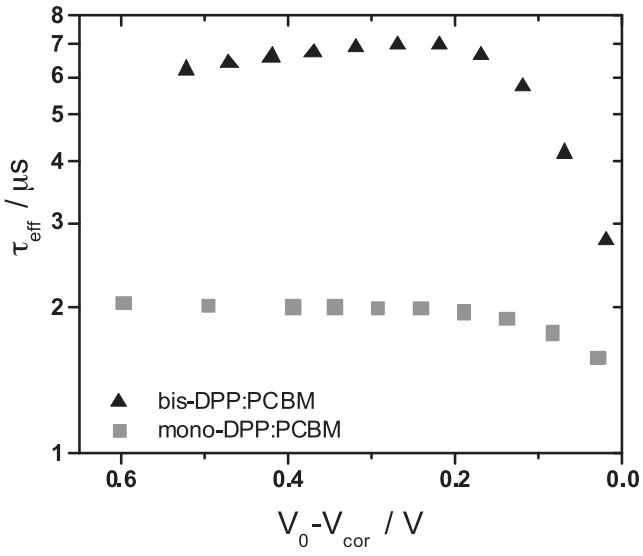

Figure 8. Effective charge carrier lifetime versus effective voltage in mono-DPP:PCBM and bis-DPP:PCBM devices measured at 100 mW/cm^2 incident light intensity.

with the intensity dependence of the photocurrent noted earlier that indicated mono-DPP:PCBM has a stronger bimolecular recombination rate. The τ_{eff} in bis-DPP:PCBM decreases sharply at low effective voltages (close to V_{oc}) falling to within a factor of two of the τ_{eff} in mono-DPP:PCBM. This may be related to a field dependent mobility[13] or increased recombination near the electrodes due to charge injection. The surprisingly weak voltage dependence for τ_{eff} in the mono-DPP:PCBM system may be indicative of a charge trapping mechanism and/or voltage dependent geminate losses. Future investigations will explore these possibilities in more detail.

We can further our analysis by considering that at open circuit all photogenerated charges recombine and therefore the generation rate, G, is equal to the recombination rate R. Maintaining the assumption that voltage dependent geminate recombination is negligible, G can be determined from the saturated photocurrent by the relation $J_{ph,sat} = qLG$.[9] As discussed in Section 2.2 the light intensity dependence of the V_{oc} indicates that bimolecular recombination dominates at open circuit in both mono-DPP:PCBM and bis-DPP:PCBM. Therefore the recombination rate at V_{oc} can be expressed as $R = \gamma n_{oc}^2$ where γ is the bimolecular recombination rate constant.[32] Coupling these relations, we estimate that at 1 sun for mono-DPP:PCBM $\gamma \approx 5.3 \times 10^{-17}$ m^{3}s^{-1} and for bis-DPP:PCBM, $\gamma \approx 2.6 \times 10^{-17}$ m^{3}s^{-1}. This corresponds to Langevin reduction factors of 0.11 and 0.03 for mono-DPP:PCBM and bis-DPP:PCBM respectively compared to the predicted γ from the Langevin model ($\gamma = q/\varepsilon(\mu_e + \mu_h)$). It is worth noting that the Langevin reduction factors found here are on the lower end of what has been reported for most polymer:fullerene systems. It has been suggested that the origin of reduced Langevin rates may be the inherent assumption that the density of holes and electrons is equal everywhere when in reality the active layer may have significant inhomogeneity in the hole and electron densities due to the separated domains of donor and acceptor materials.[51,52] Following this

© 2013 WILEY-VCH Verlag GmbH & Co. KGaA, Weinheim

reasoning, it may be that the small molecule blends studied here are more homogeneous than most polymer:fullerene blends. This topic will be the subject of future study.

2.5. Effect of Carrier Lifetime and Mobility on Solar Cell Performance

Up to this point, we have shown the mono-DPP:PCBM system exhibits a lower hole mobility and a shorter effective carrier lifetime than the bis-DPP:PCBM system. We now attempt to differentiate the influence of μ and τ_{eff} on solar cell performance. The Hecht formula[10,36,51] can be used to directly assess the effect of the $\mu\tau_{eff}$ product on Q/Q_0,the fraction of photogenerated charges which are collected before recombination. As first described by Hecht,

$$\frac{Q}{Q_0} = \frac{\mu\tau_{eff}F}{L/2}\left(1 - \exp\left(\frac{-L/2}{\mu\tau_{eff}F}\right)\right) \quad (11)$$

where $F = (V_o - V_{cor})/L$ is the electric field across the device thickness L, and $L/2$ is the average depth of photogenerated carriers assuming uniform photogeneration throughout the device. **Figure 9** shows Q/Q_0 calculated for mono-DPP:PCBM and bis-DPP:PCBM as a function of F using the lifetime data presented in Figure 8 with L = 90 nm. For the mobilities, we assume transport to be limited by the slowest carrier and input only the measured hole mobilities. The Hecht formula seems to slightly underestimate the collection efficiency for mono-DPP:PCBM, which is not surprising given the inherent assumptions of uniform photogeneration, constant electric field and fixed mobility. This may also be an indication that there are indeed field dependent geminate recombination losses. Nonetheless, the trends in Figure 9 are consistent with the experimentally measured photocurrent. Compared to bis-DPP:PCBM (triangle symbols), Q/Q_0 for the mono-DPP:PCBM system (square symbols) is highly field-dependent–only reaching towards ≈60% collection at fields equivalent to short circuit while dropping steadily at lower effective voltages. The stark contrast between the two systems illustrates the effect of the lower mobility and shorter lifetime in the mono-DPP:PCBM system. In order to separate the influences of μ and τ_{eff}, Figure 9 also includes the results of Equation (9) with a $\mu\tau_{eff}$ using the μ in bis-DPP:PCBM and the τ_{eff} in mono-DPP:PCBM (dashed-dot line) and the μ in mono-DPP:PCBM and the τ_{eff} in bis-DPP:PCBM (dashed line). In the low μ comparison (dashed line vs squares), it is clear that increasing the τ_{eff} in mono-DPP:PCBM to that measured in the high *FF* bis-DPP:PCBM system would result in a modest reduction of the carrier collection field dependence. However, the field dependence of Q/Q_0 and thus the *FF*, would still be much worse than observed in the bis-DPP:PCBM system (triangle symbols). Alternatively, increasing the mobility of mono-DPP:PCBM to that of bis-DPP:PCBM while maintaining the same τ_{eff} (dashed dot line vs triangle symbols) would have a much greater impact on the field dependence of charge collection. In this case, it appears that even with a shorter τ_{eff} mono-DPP:PCBM would show a similar field-dependence as bis-DPP:PCBM. In practice, this would lead to both an increase in *FF* and short circuit current as the photocurrent would saturate at much lower fields. Therefore, we conclude that the mono-DPP:PCBM system is primarily limited by (hole) mobility.

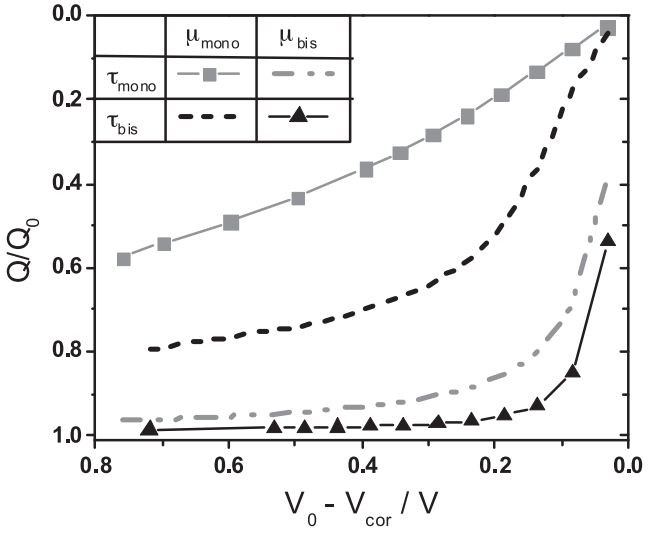

Figure 9. Ratio of generated charges versus collected charge (Q/Q_0) as a function of effective voltage for bis-DPP:PCBM and mono-DPP:PCBM calculated using the measured τ_{eff} and hole mobilities. The "mono" and "bis" subscripts in the legend correspond to mono-DPP:PCBM and bis-DPP:PCBM, respectively.

The conclusion that mobility is the primary limitation to *FF* and also limits J_{sc} in mono-DPP:PCBM devices may have broad implications for future molecular design. Indeed, the bis-DPP:PCBM mobility values reported here are similar to those reported for efficient polymer:fullerene systems with high *FF*s[20,52] while the mono-DPP:PCBM mobility is similar to other small molecule[3,5,6,53] and polymer[10,25] systems with relatively low *FF*s. This trend of mobility and *FF* has also been predicted in device simulations.[23]

Comparing the chemical structures of mono-DPP and bis-DPP suggests that extending conjugation length is one approach to enhancing charge transport properties. This may help improve π–π stacking between donor molecules yielding a more continuous network within blended films. The positive correlation between conjugation length and mobility was observed in another recent study on solution processable small molecules[56] and seems to be a successful platform for highly efficient SSMBHSCs.[1,55] Other molecular design strategies such as incorporating planar π-stacking moieties have also been shown to enhance mobility and increase *FF* in SSMBHSCs.[58] Based on these findings, we recommend that design rules for efficient charge transport be considered in the design of future donor molecules for SSMBHSCs.

3. Conclusions

In this study, we have investigated the charge transport properties and recombination mechanisms of the low *FF* mono-DPP:PCBM system and the high *FF* bis-DPP:PCBM system. Single carrier diodes indicate that while both systems have similar electron mobilities, the hole mobility in the mono-DPP:PCBM system is over one order lower than that in the

© 2013 WILEY-VCH Verlag GmbH & Co. KGaA, Weinheim

bis-DPP:PCBM system. Light intensity measurements of the *J–V* characteristics of optimized solar cells reveal that for both systems bimolecular recombination dominates at open circuit and the *FF* is limited by a nongeminate recombination mechanism. Analysis of the differential resistances and capacitances extracted from impedance measurements further illustrates the influence of carrier density dependent nongeminate recombination. The mono-DPP:PCBM system was found to have a shorter effective carrier lifetime compared to the bis-DPP:PCBM system. However, modeling the effect of the mobility-lifetime product on charge collection reveals that the low charge carrier mobility is the primary source of the highly field-dependent photocurrent in mono-DPP:PCBM devices. Increasing the hole mobility of mono-DPP:PCBM by an order of magnitude would allow for efficient charge collection at lower fields leading to significant increases in both the short circuit current and *FF*. Based on these findings, we conclude that in addition to tuning the optical absorption and energy levels of donor materials, future molecular design should aim to increase charge carrier mobility, thereby enabling faster sweep out of charge carriers before they are lost to nongeminate recombination.

4. Experimental Section

The mono-DPP and bis-DPP materials were synthesized according to previously described procedures.[4,22] The PCBM was purchased from Solenne BV and used as received. Solar cell devices and hole-only devices were fabricated by spin-casting a 40 nm PEDOT:PSS (H.C. Stark Baytron P 4083) atop Corning 1737 glass patterned with 150 nm of ITO (ShenZen NanBo Display Technology Co.) and then baking the substrates at 140 °C for 20 min. The active layers were spun cast onto the ITO/PEDOT:PSS substrates from solutions with a 1:1 donor:PCBM ratio dissolved in chloroform. The bis-DPP:PCBM solutions also contained (0.5%) 1,8-diiodooctane by volume. The solar cell device active layer thicknesses were approximately 90 nm as measured by an Ambios XP-100 Stylus Profilometer. The hole only-device active layer thicknesses were controlled by varying solution concentration (17 mg mL^{-1} to 35 mg mL^{-1}) and ranged from 100 nm to 240 nm. For solar cell (hole-only) devices, 100 nm of aluminum (gold) was deposited onto the active layer at a pressure of 10^{-6} Torr through shadow mask to form a 4.5 mm^2 electrode area. Prior to characterization, mono-DPP:PCBM devices were thermally annealed in a nitrogen atmosphere at 80 °C for 10 min. Electron only devices were made by depositing 100 nm of aluminum onto ITO substrates at a rate of 15 Å s^{-1}. Active layer blends from the same solutions used for hole only devices were then spun cast on top of the ITO/Al substrates to yield a range of thicknesses (100 nm to 200 nm). The same 4.5 mm^2 shadow masks were used while thermally evaporating 10 nm of calcium followed by 100 nm of aluminum to form the top contacts.

Solar cell device characterizations were carried out in nitrogen environment under simulated 100 mW cm^{-2} AM1.5G irradiation from a 300 W Xe arc lamp with an AM 1.5 global filter. For other illumination intensities, a Newport 5215 optical density filter wheel was placed in between the samples and the light source. The light intensity was calibrated using an NREL certified silicon diode with an integrated KG1 optical filter. Impedance measurements were conducted using a Solartron 1260 impedance analyzer under nitrogen.

Charge extraction measurements used white light LEDs with an intensity that yielded the same open circuit voltage as measured using the solar simulator at one sun. Devices were held at a fixed bias condition under illumination before the LED was switched off and a –3 V extraction bias was applied. The carrier density was determined by integrating the resulting photocurrent transient. Further details of this technique will be provided in a future publication.[50]

Supporting Information

Supporting Information is available from the Wiley Online Library or from the author.

Acknowledgements

The authors thank the Office of Naval Research for the support of this work. The material synthesis is supported by the National Science Foundation-SOLAR program (DMR-1035480). T.Q.N. thanks the Camille Dreyfus Teacher Scholar Award and the Alfred Sloan Research Fellowship program. D.N. thanks the German Science Foundation for a travel grant. C.P. thanks the National Science Foundation Graduate Research Fellowship under Grant No. DGE-1144085. The authors thank Martijn Kuik for helpful discussion. In addition, the authors thank Jona Kurpiers and Ilja Lange for assistance with the charge extraction measurements.

Received: September 12, 2012
Revised: December 27, 2012
Published online: February 25, 2013

[1] T. S. Van der Poll, J. A. Love, T.-Q. Nguyen, G. C. Bazan, *Adv. Mater.* **2012**, *24*, 3646.
[2] B. Walker, C. Kim, T.-Q. Nguyen, *Chem. Mater.* **2010**, *23*, 470.
[3] B. Walker, A. B. Tamayo, X. Dang, P. Zalar, J. H. Seo, A. Garcia, M. Tantiwiwat, T. Nguyen, *Adv. Funct. Mater.* **2009**, *19*, 3063.
[4] A. B. Tamayo, X.-D. Dang, B. Walker, J. Seo, T. Kent, T.-Q. Nguyen, *Appl. Phys. Lett.* **2009**, *94*, 103301.
[5] Z. Li, G. He, X. Wan, Y. Liu, J. Zhou, G. Long, Y. Zuo, M. Zhang, Y. Chen, *Adv. Energy Mater.* **2012**, *2*, 74.
[6] G. C. Welch, L. A. Perez, C. V. Hoven, Y. Zhang, X.-D. Dang, A. Sharenko, M. F. Toney, E. J. Kramer, T.-Q. Nguyen, G. C. Bazan, *J. Mater. Chem.* **2011**, *21*, 12700.
[7] Y. Zhang, X. Dang, C. Kim, T.-Q. Nguyen, *Adv. Energy Mater.* **2011**, *1*, 610.
[8] D. Credgington, F. C. Jamieson, B. Walker, T.-Q. Nguyen, J. R. Durrant, *Adv. Mater.* **2012**, *24*, 2135.
[9] V. D. Mihailetchi, J. Wildeman, P. W. M. Blom, *Phys. Rev. Lett.* **2005**, *94*, 126602.
[10] A. Baumann, J. Lorrmann, D. Rauh, C. Deibel, V. Dyakonov, *Adv. Mater.* **2012**, *24*, 4381.
[11] R. A. Marsh, J. M. Hodgkiss, R. H. Friend, *Adv. Mater.* **2010**, *22*, 3672.
[12] T. J. K. Brenner, Z. Li, C. R. McNeill, *J. Phys. Chem. C* **2011**, *115*, 22075.
[13] S. Albrecht, W. Schindler, J. Kurpiers, J. Kniepert, J. C. Blakesley, I. Dumsch, S. Allard, K. Fostiropoulos, U. Scherf, D. Neher, *J. Phys. Chem. Lett.* **2012**, *3*, 640.
[14] C. G. Shuttle, B. O'Regan, A. M. Ballantyne, J. Nelson, D. D. C. Bradley, J. R. Durrant, *Phys. Rev. B* **2008**, *78*, 113201.
[15] C. G. Shuttle, R. Hamilton, B. C. O'Regan, J. Nelson, J. R. Durrant, *Proc. Natl. Acad. Sci. USA* **2010**, *107*, 16448.
[16] S. R. Cowan, N. Banerji, W. L. Leong, A. J. Heeger, *Adv. Funct.Mater.* **2012**, *22*, 1116.
[17] J. Kniepert, M. Schubert, J. C. Blakesley, D. Neher, *J. Phys. Chem. Lett.* **2011**, *2*, 700.
[18] R. Mauer, I. A. Howard, F. Laquai, *J. Phys. Chem. Lett.* **2011**, *2*, 1736.
[19] G.-J. A. H. Wetzelaer, M. Kuik, P. W. M. Blom, *Adv. Energy Mater.* **2012**, *2*, 1232.
[20] A. Pivrikas, H. Neugebauer, N. S. Sariciftci, *IEEE J. Sel. Top. Quantum Electron.* **2010**, *16*, 1746.

© 2013 WILEY-VCH Verlag GmbH & Co. KGaA, Weinheim

[21] S. R. Cowan, W. L. Leong, N. Banerji, G. Dennler, A. J. Heeger, *Adv. Funct. Mater.* **2011**, *21*, 3083.
[22] Y. Zhang, C. Kim, J. Lin, T.-Q. Nguyen, *Adv. Funct. Mater.* **2012**, *22*, 97.
[23] C. Deibel, A. Wagenpfahl, V. Dyakonov, *Phys. Status Solidi RRL* **2008**, *2*, 175.
[24] N. Tessler, N. Rappaport, *Appl. Phys. Lett.* **2006**, *89*, 013504.
[25] M. M. Mandoc, W. Veurman, L. J. A. Koster, B. de Boer, P. W. M. Blom, *Adv. Funct. Mater.* **2007**, *17*, 2167.
[26] P. W. M. Blom, M. J. M. de Jong, J. J. M. Vleggaar, *Appl. Phys. Lett.* **1996**, *68*, 3308.
[27] P. N. Murgatroyd, *J. Phys. D: Appl. Phys.* **1970**, *3*, 151.
[28] N. I. Craciun, J. J. Brondijk, P. W. M. Blom, *Phys. Rev. B* **2008**, *77*, 035206.
[29] S. M. Tuladhar, D. Poplavskyy, S. A. Choulis, J. R. Durrant, D. D. C. Bradley, J. Nelson, *Adv. Funct. Mater.* **2005**, *15*, 1171.
[30] V. D. Mihailetchi, J. K. van Duren, P. W. Blom, J. C. Hummelen, R. A. Janssen, J. M. Kroon, M. T. Rispens, W. J. Verhees, M. M. Wienk, *Adv. Funct. Mater.* **2003**, *13*, 43.
[31] L. J. A. Koster, M. Kemerink, M. M. Wienk, K. Maturová, R. A. J. Janssen, *Adv. Mater.* **2011**, *23*, 1670.
[32] S. R. Cowan, A. Roy, A. J. Heeger, *Phys. Rev. B* **2010**, *82*, 245207.
[33] R. Mauer, I. A. Howard, F. Laquai, *J. Phys. Chem. Lett.* **2010**, *1*, 3500.
[34] L. J. A. Koster, V. D. Mihailetchi, R. Ramaker, P. W. M. Blom, *Appl. Phys. Lett.* **2005**, *86*, 123509.
[35] A. M. Goodman, A. Rose, *J. Appl. Phys.* **1971**, *42*, 2823.
[36] R. A. Street, M. Schoendorf, A. Roy, J. H. Lee, *Phys. Rev. B* **2010**, *81*, 205307.
[37] C. Deibel, A. Wagenpfahl, *Phys. Rev. B* **2010**, *82*, 207301.
[38] G. F. A. Dibb, T. Kirchartz, D. Credington, J. Durrant, J. Nelson, *J. Phys. Chem. Lett.* **2011**, *2*, 2407.
[39] F. Fabregat-Santiago, G. Garcia-Belmonte, I. Mora-Seró, J. Bisquert, *Phys. Chem. Chem. Phys.* **2011**, *13*, 9083.
[40] I. H. Campbell, D. L. Smith, J. P. Ferraris, *Appl. Phys. Lett.* **1995**, *66*, 3030.
[41] M. Meier, S. Karg, W. Riess, *J. Appl. Phys.* **1997**, *82*, 1961.
[42] L. Burtone, D. Ray, K. Leo, M. Riede, *J. Appl. Phys.* **2012**, *111*, 064503.
[43] P. P. Boix, A. Guerrero, L. F. Marchesi, G. Garcia-Belmonte, J. Bisquert, *Adv. Energy Mater.* **2012**, *1*, 1073.
[44] G. Garcia-Belmonte, A. Munar, E. M. Barea, J. Bisquert, I. Ugarte, R. Pacios, *Org. Electron.* **2008**, *9*, 847.
[45] W. L. Leong, G. C. Welch, L. G. Kaake, C. J. Takacs, Y. Sun, G. C. Bazan, A. J. Heeger, *Chem. Sci.* **2012**, *3*, 2103.
[46] R. A. Street, K. W. Song, S. Cowan, *Org. Electron.* **2011**, *12*, 244.
[47] A. Guerrero, T. Ripolles-Sanchis, P. P. Boix, G. Garcia-Belmonte, *Org. Electron.* **2012**, *13*, 2326.
[48] C. G. Shuttle, B. O'Regan, A. M. Ballantyne, J. Nelson, D. D. C. Bradley, J. C. de Mello, J. R. Durrant, *App. Phys. Lett.* **2008**, *92*, 093311.
[49] C. G. Shuttle, A. Maurano, R. Hamilton, B. O'Regan, J. C. de Mello, J. R. Durrant, *App. Phys. Lett.* **2008**, *93*, 183501.
[50] J. Kniepert, I. Lange, D. Neher, unpublished.
[51] C. Deibel, A. Wagenpfahl, V. Dyakonov, *Phys. Rev. B* **2009**, *80*, 075203.
[52] C. Groves, N. C. Greenham, *Phys. Rev. B* **2008**, *78*, 155205.
[53] K. Hecht, *Z. Phys.: Hadrons Nucl.* **1932**, *77*, 235.
[54] Y. Liang, Z. Xu, J. Xia, S. Tsai, Y. Wu, G. Li, C. Ray, L. Yu, *Adv. Mater.* **2010**, *22*, E135.
[55] A. B. Tamayo, B. Walker, T.-Q. Nguyen, *J. Phys. Chem. C* **2008**, *112*, 11545.
[56] C. Kim, J. Liu, J. Lin, A. B. Tamayo, B. Walker, G. Wu, T.-Q. Nguyen, *Chem. Mater.* **2012**, *24*, 1699.
[57] Y. Sun, G. C. Welch, W. L. Leong, C. J. Takacs, G. C. Bazan, A. J. Heeger, *Nat. Mater.* **2012**, *11*, 44.
[58] O. P. Lee, A. T. Yiu, P. M. Beaujuge, C. H. Woo, T. W. Holcombe, J. E. Millstone, J. D. Douglas, M. S. Chen, J. M. J. Fréchet, *Adv. Mater.* **2011**, *23*, 5359.

© 2013 WILEY-VCH Verlag GmbH & Co. KGaA, Weinheim